Published in final edited form as:

Cancer Res. 2017 September 15; 77(18): 5026–5038. doi:10.1158/0008-5472.CAN-16-2834.

An essential role for the tumor suppressor Merlin in regulating fatty acid synthesis

Dina S. Stepanova[1], **Galina Semenova**[3], **Yin-Ming Kuo**[2], **Andrew J. Andrews**[2], **Sylwia Ammoun**[4], **C. O. Hanemann**[4], and **Jonathan Chernoff**[3,5]

[1]Pirogov Russian National Research Medical University, Moscow, Russia

[2]Cancer Epigenetics Program, Fox Chase Cancer Center, Philadelphia, PA

[3]Cancer Biology Program, Fox Chase Cancer Center, Philadelphia, PA

[4]Peninsula Schools of Medicine and Dentistry, Plymouth University, Plymouth, UK

Abstract

Neurofibromatosis type 2 (NF2) is an autosomal dominant disorder characterized by the development of multiple tumors in the central nervous system, most notably schwannomas and meningiomas. Mutational inactivation of the *NF2* gene encoding the protein Merlin is found in most sporadic and inherited schwannomas, but the molecular mechanisms underlying neoplastic changes in schwannoma cells remain unclear. We report here that Nf2-deficient cells display elevated expression levels of key enzymes involved in lipogenesis and that this upregulation is caused by increased activity of Torc1. Inhibition or knockdown of fatty acid synthase (FASN), the enzyme that catalyzes the formation of palmitic acid from malonyl-CoA, drove *NF2*-deficient cells into apoptosis. Treatment of *NF2*-mutant cells with agents that inhibit the production of malonyl-CoA reduced their sensitivity to FASN inhibitors. Collectively, these results suggest that the altered lipid metabolism found in *NF2*-mutant cells renders them sensitive to elevated levels of malonyl-CoA, as occurs following blockade of fatty acid synthase, suggesting new targeted strategies in the treatment of *NF2*-deficient tumors.

Keywords

neurofibromatosis 2; schwannoma; metabolism; fatty acid synthesis; small molecule inhibitors

Introduction

Neurofibromatosis type 2 (NF2) is an autosomal dominant cancer predisposition syndrome that occurs due to inactivating mutations in the *NF2* gene. NF2 is characterized by formation of multiple low grade tumors along the peripheral nerves and in the central nervous system (1), and associated with disease manifestations that include benign schwannomas (including bilateral vestibular schwannomas, the hallmark of the disease), meningiomas, and

[5]Correspondance to: Jonathan Chernoff, Cancer Biology Program, Fox Chase Cancer Center, 333 Cottman Ave W451, Philadelphia, PA 19111, 215 728 5319, 215 728 3616 (fax), Jonathan.Chernoff@fccc.edu.

Conflicts of interest: The authors have no conflict of interests

ependymomas. Despite the benign nature of these lesions, NF2 is often fatal due to development of inoperable intracranial tumors. In addition, somatic mutations in the *NF2* gene also contribute to malignant mesotheliomas and other tumors (2). To date there is no effective pharmacotherapy for NF2 and the morbidity and mortality of this inherited disorder remains high.

The *NF2* gene product, merlin, is a member of the ezrin-moesin-radixin protein family and functions to regulate cell adhesion via receptor tyrosine kinases and integrins (3–7), proliferative and survival signaling via enzymes such as Rac, PAK, AKT, FAK, and MTOR (8–11), and to suppress tumorigenesis via inhibition of the E3 ubiquitin ligase CRL4/DCAF1 complex (12). In addition, Merlin signaling may also impact the MST/YAP contact inhibition signaling pathway (13). Loss of *NF2* gene leads to inability of cells to form stable cell:cell junctions (14), and *NF2*-deficient cells do not show contact growth inhibition (4,14). Conversely, Merlin overexpression blocks proliferation (15).

Currently, three targeted therapeutic approaches are being investigated for potential use in NF2: angiogenesis inhibitors such as bevacizumab (16,17), EGFR inhibitors such as erlotinib and lapatinib (18), and MTOR inhibitors such as sirolimus and everolimus (19). While the use of such targeted agents has shown promise in early trials, the redundancy of proliferative, survival, and motility signaling cascades in Merlin-null cells suggests a need to identify additional therapeutic concepts and targets in this disorder.

Recently, there has been revived interest in targeting metabolic enzymes in various malignancies. Most of these efforts have attempted to exploit unique aspects of sugar metabolism in cancer, the so-called Warburg effect. However, cancer cells also require large amounts of lipid for membrane biosynthesis, energy, and signal transduction and such lipids are supplied by *de novo* fatty acid synthesis (20). Accordingly, enzymes involved in fatty acid metabolism, such as fatty acid synthase (FASN), are commonly upregulated in cancer cells, and inhibiting FASN or other enzymes involved in lipogenesis can induce apoptosis in such cells (21,22). These data show that enzymes involved in lipid metabolism are potential therapeutic targets against cancers.

In this report, we used *Nf2*-deficient *vs.* WT cells to screen for metabolic changes caused by *Nf2* gene loss. We found that *Nf2*-deficient fibroblasts and Schwann cells display a variety of metabolic derangements involving lipid metabolism, in particular, a significant elevation of fatty acid levels. Further studies showed that *Nf2*-deficient cells are selectively sensitive to inhibitors of fatty acid synthase (FASN). We report that siRNA or small molecule inhibitors of FASN are toxic to *Nf2*-deficient cells, and that this toxicity appears to be related to a build up of pro-apoptotic metabolic intermediates, in particular malonyl-CoA. Our findings define a new aspect of NF2 pathobiology that could be used to identify therapeutic agents in this syndrome.

Methods

Plasmids, antibodies, and reagents

pBabe-NF2 was obtained from Addgene. Anti-*Fasn* siRNA (M-040091-01-0005), anti-*Acaca* siRNA (M-063938-01-0005), anti-*Mtor* (M-065427-00-0005), anti-*Rptor* (M-058754-01-0005), anti-*Rictor* (M-064598-01-0005) and non-silencing (D-001206-13-05) siRNA were purchased from Dharmacon. Individual siRNAs against *Mtor* (SASI_Mm01-00164496 and -00164492), *Rictor* (-00137732 and -00137730), *Rptor* (-00055298 and -00334580), *Fasn* (-00177858 and -00177854), *Acaca* (-0011590 and -00115905), and *Mlycd* (-00028572 and -00028576) were purchased from Sigma-Aldrich. Anti-Merlin antibodies were purchased from Abcam (#ab88957). Lipid synthesis and metabolism antibody kit (includes anti-Fasn, -phospho ACC, -ACC, -Lipin1, -ACLY, -phospho ACLY, -ACSL1, and -ACECS1 antibodies), and anti-Casp3 antibodies were purchased from Cell Signaling Technology. Anti-SREBP1 antibodies were purchased from Santa Cruz Biotechnology. Anti-GAPDH antibodies were purchased from EMD-Millipore.

Cerulenin, C75, luteolin, 5-(tetradecyloxy)-2-furoic acid (TOFA) and 5-iodotubercidin were purchased from Enzo Life Sciences. GSK2194069, dimethylsulfoxyde (DMSO), staurosporin, sodium palmitate, 70% perchloric acid, ammonium formate, acetonitrile, acetyl-coenzyme A lithium salt, malonyl coenzyme A lithium salt, propionyl-coenzyme A lithium salt, and poly-L-lysine were purchased from Sigma-Aldrich.

Cell culture

DMEM, DMEM/F12, PBS, N2 supplement, 0.05% trypsin, and Alamar Blue were purchased from Life Technologies. Fetal bovine serum was purchased from Atlanta Biologicals, heregulin-1 from R&D Systems, forskolin and laminin from EMD Millipore, and the WST-1 assay kit from Clontech.

Nf2$^{f/f}$ mouse embryo fibroblasts (MEFs) carrying flox site in exon 2 of *Nf2* gene (23), FC912 (*Nf2*$^{f/f}$) mouse Schwann cells, FH912 (*Nf2*-deficient) mouse Schwann cells, and SC4-9 (*Nf2*-deficient) mouse schwannoma cells were a generous gift of Dr. Marco Giovannini (House Ear Institute, CA), obtained in 2012. RT4 rat schwannoma cells were obtained from ATCC in 2012. All cell lines except FH912 and FC912 were grown in DMEM GlutaMAX with high glucose, 1 mM sodium pyruvate, 0.1 mM non-essential amino acids and 10% FBS at 37°C, 5% CO_2. FH912 and FC912 cells were grown in DMEM:F12 with 2 mM forskolin, 10 ng/ml heregulin, and N2 supplement on laminin-poly-L-lysine coated plates. MEF *Nf2*$^{f/f}$ cells were immortalized with pMSE-SV40LT plasmid. Deletion of the *Nf2* gene from MEF *Nf2*$^{f/f}$ cells was achieved by transfecting these cells with a pMSCV-Cre-GFP plasmid and sorting for GFP-positive cells. Cell line authentication was confirmed by two methods. First, *Nf2* deletion was confirmed by PCR genotyping and by immunoblotting (data not shown). Second, the species of origin was confirmed by short tandem repeat profiling. For the reexpression of merlin in *Nf2*-deficient schwannoma cells SC4-9 cells were transiently transfected with pBabe-NF2-puro plasmid. Control cells were transfected with pBabe-puro plasmid. Merlin expression level was detected by

immunoblotting (Fig. S1). Untreated plates for growth control were grown in parallel with experimental plates.

Cells were grown in 10-cm culture plates for no longer than 30 passages and allowed to grow for 3–4 passages after thawing before the actual experiments started. Each cell line was tested for mycoplasma upon thawing every new vial of cells (at the time of 3d passage after thawing) using mycoplasma growth indicator cultures of Vero cells, detected by fluorescence microscopy using the DNA-specific fluorochrome Hoeschst 33258. Proliferation studies were done in 96-well plates with initial cell density 104 cells/well. Immunoblotting was done in 6-well plates with initial density 2.5 × 105 cells/well. For lipogenesis-related protein immunoblotting cells were grown in serum-free conditions. For mitochondrial respiration assay cells were grown in 96-well plates provided with the analyzer at initial density 4×10^3 cells/well. For RNA extraction cells were grown in 6 cm culture plates until confluent in serum-free conditions. For UPLC-MS/MS and metabolomic studies cells were grown in 30 cm culture plates until confluent.

Primary schwannoma cell cultures: After informed consent, human primary schwannoma tissue samples were collected during operations at Derriford Hospital (Plymouth, UK) or Southmead Hospital (Bristol, UK) under local R&D approval Plymouth Hospitals NHS Trust: R&D No: 14/P/056 and North Bristol NHS Trust: R&D No: 3458. All patient studies were conducted in accordance with the Declaration of Helsinki under IRB approval. Cells were isolated by digestion using a mixture of collagenase, dispase and mechanical digestion by pipetting. Once digested cells were cultured in growth factor medium (GFM): DMEM, 10% FBS, 100U/ml pen/strep; 0.5μM Forskolin; 2.5 μg/ml Amphotericin; 2.5 μg/ml Insulin; 10 nM β1 heregulin, maintained in a humidified atmosphere of 10% CO2 at 37ºC on plates coated with both poly-L lysine and laminin. Human schwannoma primary cells (passages 1–4) and used in this study are Merlin-negative. All Schwann cell cultures are S100 positive.

Primary meningioma and Human meningeal cell (HMC, Catalog #1400, ScienCell Research Laboratories) cultures: All the meningioma tumor samples used were collected under the MOT project involving both Derriford and Southmead Hospitals. The project was granted full ethics approval by the South West research ethics committee (REC number 14/SW/0119). All tumors used in this project were classified as WHO grade 1. Meningioma cells were isolated using a mixture of collagenase, dispase and mechanical digestion by pipetting. Once digested Meningioma cells were grown in DMEM containing glucose (4.5 g/l), 10% FBS, 100 U/ml penicillin/streptomycin and 1% glutamine. Human meningeal cells (HMC, Sciencell, CA, USA) were grown in the recommended HMC medium (Sciencell) at 37 °C and 5% CO2. Human meningioma grade I primary cells (passages 1–4) used in this study are Merlin-negative.

All primary cells were grown in Mycoplasma ExS (PromoCell GmbH, Heidelberg, Germany) treated incubators. No additional mycoplasma testing was performed.

Proliferation and viability assays

Proliferation and viability were evaluated by Alamar Blue reagent according to the manufacturer’s protocol. For the human schwannoma and meningioma samples

immunofluorescence proliferation and viability assays were performed: cells were cultured for 72 h in GFM with or without GSK2194069 (0.1, 1 and 10 μM). Pre-treated cells were fixed using 4% paraformaldehyde (PFA) and permeablised using 0.2% Triton X-100 before being blocked using 10% normal goat serum. Cells were then incubated with primary antibodies overnight at 4° C at a concentration of 1:100 in 1%BSA Phosphate-buffered saline (PBS). Anti-Ki67 (Dako) was used as a marker or proliferating cells and anti-cleaved caspase-3 (Cell Signalling Technologies) was used as a marker or cells undergoing apoptosis. AlexaFluorTM secondary antibodies goat-anti mouse 594 and goat-anti rabbit 488 were used and DAPI applied as a nuclear stain.

Confocal Microscopy: Multitrack imaging was performed using a Zeiss Confocal LSM510. Proliferation and survival assays which were carried out using a 20x air objective. The appropriate Zeiss image manipulation software (ZEN) was used for editing.

Transfections were done by electroporation using Neon transfection system (Life Technologies, Grand Island, NY) according to manufacturer's protocol. Transfections were done in 100 μL tips. For DNA transfections final concentration of 5 μg per reaction was used. For RNA transfections final concentration of 100 nM was used.

Immunoblotting

Cells were lysed with RIPA (1% Triton-X100; 10% glycerol; 50 mM HEPES, pH 7.4; 150 mM NaCl; 1.5 mM $MgCl_2$, 1 mM EGTA, 1 mM EDTA, 0.1% SDS, 10 mM phenylmethylsulphonyl-fluoride; aprotinin 10 μg/mL, leupeptin 10μg/mL, pepstatin 10 μg/mL, 10 mM sodium fluoride) for 15 min. on ice. Proteins of interest were detected by regular immunoblotting using a Lipid synthesis and metabolism antibody kit, anti-cleaved Casp3 rabbit monoclonal antibody, and mouse anti-merlin, anti-βActin, anti-Srebp1 and anti-Gapdh antibodies. Goat anti-rabbit HRP-conjugated and anti-mouse AP-conjugated immunoglobulins were used with Western Chemiluminescent HRP Substrate (Millipore, Billerica, MA) and ImmunStar AP substrate (Bio-Rad, Hercules, CA). Bands were visualized on FluorChem™ E System (ProteinSimple, Santa Clara, CA) and analyzed using ImageJ software. Band intensities were normalized to Gapdh or β-Actin band intensities.

qPCR

Cells were grown in serum-free media in 6-cm plates until confluent, and total RNA was extracted using RNeasy Minikit (Qiagen, Valencia, CA). Quantitative RT-PCR reactions were performed using TaqMan probes and primers designed by the manufacturer, using an ABI PRISM 7700 detection system (Applied Biosystems, Foster City, CA). Results were analyzed using relative standard curve method. For *Acacb* comparative Ct method was used. The average of *Hprt1, Tbp* and *Actinb* expression was used for normalization. See Supplemental data for the complete list of primers.

Acyl-CoA quantification

4 types of samples were analyzed: and MEF $Nf2^{-/-}$, treated with DMSO, MEF $Nf2^{-/-}$, treated with cerulenin, MEF $Nf2^{f/f}$, treated with DMSO, and MEF $Nf2^{f/f}$, treated with cerulenin. ~1 g of cell pellet per sample type was used for analysis. Propionyl-CoA was used

as a recovery standard. After the solid phase extraction acidified and neutralized samples were put to the Waters Acquity H-class ultra-high performance liquid chromatography (UPLC, Milford, MA) with the isocratic mobile phase: 50 mM ammonium formate:acetonitrile (30:70, v/v). The eluates were directly introduced into the coupled Thermo triple quadrupole mass spectrometer (TSQ Quantum Access, Waltham, MA) for quantitative analysis. See Supplemental data for the complete procedure description.

Mitochondrial respiration measurement

The study was performed in a 96-well format on a Seahorse XF analyzer using Seahorse Mito Stress Kit (Seahorse Bioscience, N. Billerica, MA, USA) according to the manufacturer's protocol. Initial cell density was 4×10^3 cells/well. Upon assay completion cells were lysed and used for protein concentration assay (Bradford). All data was normalized to protein concentrations.

Animal studies

All animal procedures were performed in accordance with IACUC guides and regulations. Mouse schwannoma xenografts were performed on female *nu/nu* mice, n=5. 3×10^6 SC4-9 cells in matrigel per mouse were injected subcutaneously. A 100x stock solution of cerulenin was prepared in DMSO:ethanol (1:4) and stored at −20 °C. A working solution in corn oil was prepared daily and given by oral gavage at a dose of 30 or 2 mg/kg/day (cerulenin) and 3 mg/kg/day (GSK2194069) starting day 3 after injection. Mice were sacrificed by cervical dislocation after 4 weeks of treatment.

Metabolic studies

6 groups of samples were analyzed: non-treated *Nf2*-deficient mouse Schwann cells FH912 and wild type mouse Schwann cells FC912; non-treated $Nf2^{-/-}$ and $Nf2^{f/f}$ MEFs; and $Nf2^{-/-}$ and $Nf2^{f/f}$ MEFs treated with 5 μM cerulenin for 24 hours. 5 samples per sample type were prepared according to Metabolon sample preparation guidelines (Metabolon Inc., Durham, NC).

Half inhibitory concentration (IC_{50})

Drugs were added to the cells 4 hours after plating and incubated for 48 hours. For *Acaca* knockdown C75 was added next day after transfection and incubated for 48 hours. IC_{50} was calculated by the following formula: $IC_{50}=a+b*arctg(1-1/2c)$ after minimization of quadratic distance between experimental data and a fit curve $y=c*(1-tg((x-a)/b))$, where x is the drug concentration, by modifying coefficients a, b and c.

Statistical analysis

All IC_{50} studies were done in quadruplicates and repeated 4 times. *Fasn* and *Acaca* knockdown and ACC1 chemical activation and inhibition experiments were done in quadruplicates and repeated 3 times. *Mlycd* knockdown was done in quadruplicates and repeated 4 times. Lipogenesis immunoblotting and qPCR studies were repeated 4 times. MTOR signaling and MTOR inactivation experiments were repeated 2 times. UPLC-MS/MS studies were repeated 3 times. Mean values and confidence interval 95% were used

to build graphs. Statistical significance p was determined by two-tailed Student's t-test with Welch's correction for increased Casp3 cleavage studies, UPLC-MS/MS, and for *in vivo* studies; and by Holm-Sidak method with α=5% for lipogenesis immunoblotting and qPCR studies. For the schwannoma xenograft FASN expression p-value was calculated by Mann-Whitney test. For human schwannoma samples ANOVA was used. Experiments were performed in at least triplicates using at least three independent batches of cells from different individuals. In a figure, mean ± s.e.m. is given.

Results

Metabolic profiling of *Nf2*-deficient cells

We performed metabolic profiling of *Nf2*-deficient MEFs and Schwann cells (FH912) in comparison with WT MEFs ($Nf2^{f/f}$) and Schwann cells (FC912) to see if metabolic pathways were altered by loss of the *Nf2* gene. Metabolite profiling showed a broad spectrum of changes in *Nf2*-deficient cells. Specifically, we observed elevated levels of tricarbonic acid (TCA) cycle metabolites in $Nf2^{-/-}$ MEFs (Table 1) and increased levels of long chain and branched fatty acids in both FH912 Schwann cells and $Nf2^{-/-}$ MEFs (Table 2), consistent with increased energy demand in these cells (24–26). An increase in vitamins and cofactors levels was also observed (Table S1), especially, nicotinate metabolites involved in electron chain transport (NAD^+, NADH, and NADP) and pantothenate metabolites involved in coenzyme A turnover, consistent with an increased energy production in *Nf2*-deficient cell lines (27). In addition, the level of metabolites associated with glycolysis was decreased in both FH912 Schwann cells and $Nf2^{-/-}$ MEFs (Table 1), as well as a drop in amino acids, including particularly glutamine metabolites (Table S2), suggesting upregulated glutaminolysis supporting the more active TCA cycle. The most profound metabolic alteration, however, was the marked elevation of fatty acid levels in both FH912 cells and $Nf2^{-/-}$ MEFs (Table 2).

Loss of the *Nf2* gene renders cells vulnerable to FASN inhibitors

Since metabolic profiling indicated elevated fatty acid metabolism in $Nf2^{-/-}$ cells, we asked if these cells were sensitive to small molecule inhibitors of FASN. We found that the FASN inhibitor cerulenin (28) showed consistent selective toxicity against *Nf2*-deficient MEFs with IC_{50} ratio of 0.436±0.09, p=4E-10 (Fig. 1A). The schwannoma cell lines SC4–9 and RT4 were also sensitive to similar levels of this compound. Re-expression of Merlin in SC4–9 cells rendered these cells insensitive to cerulenin (almost two-fold difference in IC_{50} values, $p < 0.0001$) (Fig. 1B), indicating that the sensitivity to cerulenin is related to Merlin expression (Merlin expression level is shown on fig. S1A). To ensure that the observed effects were related to FASN inhibition, we asked if $Nf2^{-/-}$ MEFs were more sensitive than $Nf2^{f/f}$ MEFs to knockdown of *Fasn*. $Nf2^{-/-}$ and $Nf2^{f/f}$ MEFs were transfected with pooled anti-*Fasn* siRNA or control non-silencing siRNA. Within 24 hours, rounded apoptotic cells were observed in $Nf2^{-/-}$ cells transfected with anti-*Fasn* siRNA, but not in the control cells or in transfected $Nf2^{f/f}$ MEFs. We observed a significant increase of Casp3 cleavage in anti-*Fasn* siRNA-transfected (4.14-fold, p=0.0001) $Nf2^{-/-}$ MEFs, but not in similarly treated $Nf2^{f/f}$ MEFs (Fig. 1C and S1B). Low dose cerulenin treatment also decreased levels of FASN at some degree, and the same trend of cleaved Casp3 increase was observed in $Nf2^{-/-}$

MEFs (2.01-fold, p=0.022). The same pattern was observed when individual oligos against *Fasn* and GSK2194069 inhibitor were used (fig. S1C). We also tested the sensitivity of $Nf2^{f/f}$ and $Nf2^{-/-}$ MEFs to three additional small molecule FASN inhibitors: GSK2194069 (29), C75 (25), and Luteolin (25). In each case, loss of *Nf2* was associated with higher sensitivity to the FASN inhibitors (Fig. 1D–1F).

We next performed xenograft studies on female *nu/nu* mice using SC4–9 cells. Xenografts were placed in the flanks and the mice were treated with cerulenin (30 mg/kg/day), GSK2194069 (3 mg/kg/day), or vehicle for 28 days. As shown in Figure 1G, treatment with GSK2194069 caused a nearly two-fold reduction in tumor growth (p=0.0049), and cerulenin treatment caused a three-fold reduction (p=0.00039), consistent with the notion that inhibiting FASN represents a potentially effective strategy for NF2. At the dose given mice tolerated treatment well and did not experience weight loss or skin dryness. Remarkably, much lower doses of cerulenin (2 mg/kg/day) also effectively slowed down the tumor growth (Figure S1D). As has been reported previously (30) treatment with cerulenin was associated with a significant FASN expression decrease detected by immunoblotting of the tumor samples (Fig. S1D).

Human primary schwannoma and meningioma cells exhibit similar sensitivity to FASN inhibition

To test whether normal FASN functioning was crucial for human schwannomas and meningiomas as well as for mouse tumors we tested a series of GSK2194069 concentrations on primary human schwannoma and meningioma cells obtained from the tumor samples in comparison to normal human Schwann and meningeal cells. Primary human schwannoma cells showed similar sensitivity compared to $Nf2^{-/-}$ MEFs and mouse schwannoma SC4–9 (IC_{50} 0.68 ± 0.26 μM vs 0.19 ± 0.45 μM and 0.3 ± 0.09 μM, respectively) (Fig. 2A). Remarkably, normal Schwann cells turned to be virtually insensitive to GSK2194069 (Fig. 2A). Primary human meningioma cells also displayed similar sensitivity to the compounds, while normal human meningeal cells (HMC) were much less sensitive (IC_{50} 2.77 ± 1.57 μM vs 28.79 ± 15.86 μM, respectively) (Fig. 2B).

Reversal of the cerulenin effect by blockade of malonyl-CoA synthesis

FASN catalyzes production of palmitic acid, an essential building block for long-chain fatty acids (28,31). By inhibiting FASN, cerulenin blocks the malonyl-CoA condensation step of fatty acid synthesis, causing a deficit in palmitic acid as well as an accumulation of malonyl-CoA (26,32–35). The toxicity of malonyl-CoA in cancer cells is thought to be mediated by inhibition of carnitine palmitoyltransferase 1-regulated fatty acid β-oxidation, in turn promoting the accumulation of the sphingolipid ceramide followed by the induction of the pro-apoptotic genes such as *BNIP3*, *TRAIL* and *DAPK2*, effectors in the ceramide-mediated apoptotic pathway (36).

To evaluate the possibility that cerulenin effects in $Nf2^{-/-}$ cells might be related to reduced palmitic acid availability, we supplemented the growth media of $Nf2^{-/-}$ and $Nf2^{f/f}$ cells with palmitic acid. This addition did not reverse the toxicity of cerulenin (Fig. 3A). We next considered whether lack of fatty acid precursors or accumulation of malonyl-CoA might

promote cell death in cerulenin-treated *Nf2*$^{-/-}$ cells. We therefore knocked down acetyl-CoA carboxylase 1 (ACC1, encoded by *Acaca*), which catalyzes production of malonyl-CoA from acetyl-CoA to provide building blocks for FASN (Fig. 3B), together with cerulenin treatment. Knockdown of *Acaca* led to a striking reduction in cerulenin- and GSK2194069-induced toxicity (Fig. 3C and S2A–B). Conversely, we tested the effect and knockdown of malonyl-CoA decarboxylase (MCD, encoded by *Mlycd*) which catalyzes the conversion of malonyl-CoA back to acetyl-CoA (37). *Mlycd* knockdown increased the sensitivity of both cell lines to cerulenin and GSK2194069 (Fig. 3D and S2C). Chemical inactivation of ACC1 by 5-(tetradecyloxy)-2-furoic acid (TOFA) had a similar effect as *Acaca* knockdown (Fig. 3E), consistent with the idea that elevated levels of malonyl-CoA are toxic to these cells, and suggesting that *Nf2*$^{-/-}$ cells produce more malonyl-CoA than *Nf2*$^{f/f}$ cells. Treatment with an ACC activator, 5-iodotubercidin, which blocks an AMP kinase mediated inhibitory phosphorylation of ACC1 (38), caused an increase in cerulenin toxicity in *Nf2*$^{f/f}$ cells, but had little effect on cerulenin toxicity in *Nf2*$^{-/-}$ cells (Fig. 3F). To determine if malonyl-CoA levels actually differ according to NF2 status, we performed UPLC-MS/MS measurements of intracellular acetyl-CoA and malonyl-CoA in *Nf2*$^{-/-}$ and *Nf2*$^{f/f}$ cells (Fig. 3G). These studies showed 50% higher level of acetyl-CoA in non-treated *Nf2*$^{-/-}$ cells compared to non-treated *Nf2*$^{f/f}$ cells (p=0.0497), and a significant increase of both acetyl-CoA (by 47%, p=0.0003) and malonyl-CoA (by 90%, p=0.0002) in cerulenin-treated *Nf2*$^{-/-}$ cells, but not in cerulenin-treated *Nf2*$^{f/f}$ cells.

Upregulated lipogenesis in *Nf2*-deficient cells

Consistent with the metabolic profiling data that showed higher levels of fatty acids in *Nf2*$^{-/-}$ cells (Table 2), the selective toxicity of cerulenin appeared to be related to a greater accumulation of intermediate fatty acid synthesis products in *Nf2*$^{-/-}$ cells, and we hypothesized that the loss of *Nf2* gene might cause a general increase in lipogenesis. We found markedly elevated levels of several key lipogenesis-related proteins in *Nf2*$^{-/-}$ relative to *Nf2*$^{f/f}$ cells, including ACC-1 (45%, p=0.003) and −2 (32%, p=0.002), FASN (60%, p=0.0007), SREBP1 (71%, p=0.0001), Lipin1 (63%, p=0.0001), ACL (52%, p=0.0137), and its phosphorylated active form (69%, p=0.0012), ACECS1 (59%, p=0.0022), and ACSL1 (60%, p=0.0006). In addition, we found decreased Ser79 phosphorylation of ACC (59%, p=0.0032) in *Nf2*$^{-/-}$ MEFs, an indicator of high activity, as phosphorylation at this site inhibits ACC activity (39) (Fig. 4A and S3). Importantly, reintroduction of Merlin in SC4–9 cells decreased levels of these proteins and restored phosphorylation of ACC (Fig. 4B and S4). Consistent with the immunoblot data, quantitative PCR also showed significantly higher expression of lipogenesis-related genes in *Nf2*$^{-/-}$ MEFs relative to *Nf2*$^{f/f}$ MEFs ($p < 0.001$ for all the genes studied) (Fig. 4C). The same trend was observed in SC4–9 cells compared to SC4–9-merlin cells (Fig. 4C). Such an increase, especially of transcription factors SREBP1 and Lipin1, is consistent with our idea of upregulated lipid metabolism in *Nf2*-deficient cells. The modest effect of 5-iodotubercidin on *Nf2*$^{-/-}$ cells (Fig. 3F) is consistent with the low phosphorylation, and thus high activity, of ACC in these cells (Fig. 4A). Fig. 4D shows additional lipogenic enzyme roles in the fatty acid synthesis. *Fasn* and *Acaca* expression is controlled mainly by the transcription factor Sterol regulatory element binding protein 1 (SREBP1) (40,41), and Lipin1 is a major expression regulator of the rest of lipogenic enzymes (42,43).

Torc1 signaling is essential for fatty acid synthesis regulation

It has been previously shown that Merlin inhibits MTOR (44). MTOR is a known metabolic sensor and has been shown to regulate SREBP1 (45) and Lipin1 (46). We hypothesized that activated MTOR in *Nf2*-deficient cells might cause the upregulation of fatty acid synthesis via upregulation of SREBP1 and Lipin1. We confirmed increased MTOR phosphorylation at serine 2448 in *Nf2*-deficient MEFs (Fig. 5A) and tried chemical and siRNA inactivation of MTOR in *Nf2*-null and WT MEFs. Chemical inactivation of MTOR either by the dual TORC1 and TORC2 inhibitor Torin1 or by the TORC1 inhibitor Everolimus led to a significant reduction of the cerulenin toxicity in $Nf2^{-/-}$ MEFs (1.5-fold difference in IC_{50} values, $p = 0.027$ and 0.0064 respectively), but had a non-significant effect on WT MEFs (Fig. 5B). Immunoblot confirmed a drop in a triglyceride synthesis regulator Lipin1 and a FASN positive regulator SREBP1 protein levels caused by a decrease of MTOR phosphorylation at serine 2448 (Fig. 5B). The same effect was observed for RNAi knockdown of *Mtor* and TORC1 component *Rptor*, but not TORC2 component *Rictor* (Fig. 5C and S5A-B). Thus, a key event causing fatty acid synthesis upregulation in *Nf2*-deficient cells is TORC1 activation in the absence of Merlin.

Discussion

In this study, we show that cerulenin, an inhibitor of fatty acid synthesis is selectively toxic in cell lines lacking Merlin expression. Cerulenin has activity as an anti-obesity agent (21,47), but has also shown *in vitro* efficacy against the proliferation of colon (22), breast (48) and prostate cancer cells (21). Such sensitivity of certain cancer cells to this drug may be due to higher fatty acid synthesis levels compared to normal cells (24–26). Our findings showed that, despite their benign nature, Merlin-null cells have markedly elevated levels of fatty acid synthesis. Such cells displayed significantly higher levels of FASN and also ACC1 and 2, the enzymes that catalyze production of malonyl-CoA from acetyl-CoA. Moreover, *Nf2*-deficient cells had low levels of ACC phosphorylation, indicating high activity of this enzyme (39). The higher level of ACC expression is consistent with the pronounced rescue effect of TOFA, an ACC inhibitor, on cerulenin-treated $Nf2^{-/-}$ MEFs (Fig. 4E). FASN inhibitors have previously been shown to reduce proliferation of human malignant mesothelioma cells (49), which are often characterized by loss of function mutations in *CDKN2A/p14(ARF)* and *NF2*. Gabrielson *et al.* reported that Fasn is overexpressed in 22 of 30 human mesothelioma tissue samples compared with normal tissues, including mesothelium (49). They found that the growth of orthotopic xenografts of malignant mesothelioma cells was strongly inhibited in mice treated with the Fasn inhibitor C75. In addition, Haase *et al.* reported that Fasn expression was elevated in 70% of atypical grade II and anaplastic grade III meningiomas, and that treatment with cerulenin significantly decreased *NF2*-null meningioma cell survival *in vitro* and reduced tumor volumes in xenografts (50). These results, combined with our data in *Nf2*-null MEFs and Schwann cells, suggest that changes in lipid synthesis may be a general function in cells lacking Merlin.

Inhibitors such as cerulenin have also shown to have efficacy in a number of non-NF2 related cancer cell types *in vitro* and in preclinical models (24). In some cases, it has been proposed that these effects are mediated by targets other than FASN. For example, cerulenin

induces apoptosis in melan-a cells, but these effects appear to be independent of Fasn inhibition, and are instead thought to be mediated by an oxidative stress-associated mechanism that ultimately results in mitochondrial dysfunction (51). FASN inhibitors have also been shown to affect the activity level of the HER2/PI3K/AKT signaling pathway in U2OS cells (52). However, in our studies in the setting of Merlin deficiency, similar cellular and metabolic effects were seen with other three distinct small molecule FASN inhibitors as well as with *Fasn* siRNA. Thus, we believe that the effects of cerulenin on Merlin-null cells are related to FASN inhibition, with subsequent build-up of toxic intermediates such as malonyl-CoA, as opposed to off-target effects. This supposition is supported by the loss of cerulenin toxicity in Merlin-null cells when an ACC inhibitor is also added to the cells (Fig. 3E).

As a clinical agent, cerulenin suffers from relatively poor bioavailability. In addition, this compound, as well as the synthetic analog C75, has undesirable side effects that include anorexia and weight loss, most likely due to effects on production of neuropeptide Y in the hypothalamus as well as activation of mitochondrial fatty acid oxidation (24,47,53). In our experiments, mice tolerated treatment well, and did not experience weight loss. Still, a decrease in the FASN levels of cerulenin-treated tumors indicates that the drug reached its target in the in vivo studies. Unfortunately, the quality of antibodies against lipogenic enzymes did not allow to confirm their downregulation in the xenograft experiments, and the size of the treated tumors was too small for the HPLC analysis. It is possible that combining Fasn inhibitors with inhibitors of malonyl-CoA decarboxylase or inhibitors of AMP kinase (resulting in ACC activation and accumulation of malonyl CoA), would show additive or synergistic effects *in vivo*. We showed that activation of MTOR at Ser 2448 in *Nf2*-null cells is a key element in lipogenesis upregulation in such cells (Fig. 5A–C). As FASN expression is regulated by the transcription factor sterol regulatory element-binding protein 1c (SREBP1c) via the ERK and PI3K/AKT/MTOR pathways (54,55), modulators of these signaling pathways might also be reasonable candidates to combine with FASN inhibitors.

While our findings suggest that upregulated fatty acid synthesis is a key element in cerulenin selectivity against *Nf2*-deficient cell lines, we also found other metabolic changes that might be useful in designing targeted therapies. For example, we found a significant increase in mitochondrial respiration rate and a drop in glycolysis metabolites in both FH912 ($Nf2^{-/-}$) Schwann cells and $Nf2^{-/-}$ MEFs (Table 1 and Fig. S6). Thus, *Nf2*-deficient tumor cells differ in their utilization of glucose compared to typical malignant cancer cells, which are often characterized by aerobic glycolysis. Interestingly, $Nf2^{-/-}$ and control MEFs react differently to cerulenin treatment (Table S3). While cerulenin causes an increase in TCA metabolite level in normal cells, *Nf2*-deficient cells retain the same level of TCA metabolites. We speculate that normal cells compensate a decrease of energy production from fatty acid oxidation in the presence of cerulenin by upregulating Krebs' cycle. As $Nf2^{-/-}$ MEFs do not demonstrate such compensation it suggests there might be an initial fatty acid oxidation impairment in these cells. This supposition is also indirectly confirmed by the decrease in fatty acid oxidation gene expression in *Nf2*-deficient cells (Fig. S7). Additionally, we noted a profound drop in amino acid levels, especially in glutamate metabolites, dipeptide, and polypeptide levels in *Nf2*-null cells (Table S2). Such a general decrease in amino acid and peptide levels might indicate an increased demand of building

blocks for protein synthesis, which is likely related to the increased growth rate of *Nf2*-deficient cells. Similarly, a drop in glutamine level might be evidence of increased glutaminolysis supporting an increased energy demand. It is also of potential interest that *Nf2*-deficient cells showed an increased level of coenzymes (Table S1). This change specifically affected pantothenate and phosphopantetheine levels, and NAD^+ and NADH levels. Pantothenate and phosphopantetheine are essential for coenzyme A synthesis, and elevation of their levels is an indication of higher lipid, carbohydrate, and amino acid metabolism rates (56). Such an increase in NAD^+ and NADH levels is likely necessary to support greater energy metabolism in *Nf2*-deficient cells.

In summary, we have shown for the first time that *Nf2*-deficiency is associated with a profound reprogramming of cellular metabolism, favoring biosynthetic processes and limiting catalytic processes, and that this altered metabolism might be exploited therapeutically. In particular, the increased dependence of *Nf2*-deficient cells on lipid synthesis suggests that Fasn inhibitors, alone or in combination with other agents that increase malonyl-CoA levels, might be useful in treating NF2-related diseases.

Supplementary Material

Refer to Web version on PubMed Central for supplementary material.

Acknowledgments

Funding support: This work was supported by grants from the NIH (R01 CA148805), DOD (NF050032, NF130108) and CTF to J. Chernoff, and from the NIH (P30 CA006927) to the Fox Chase Cancer Center, a gift from the Galloway family, as well as by an appropriation from the state of Pennsylvania. Human schwannoma and meningioma studies were supported by the Brain Tumor Research charity to C.O. Hanemann.

We thank Dr. Tyler Jacks (Koch Institute for Integrative Cancer Research at MIT) for the pBabe-NF2 plasmid; Dr. Marco Giovannini (House Ear Institute) for $Nf2^{f/f}$ MEFs, and SC4–9, FH912 and FC912 Schwann cells; Dr. Emmanuelle Nicolas (Fox Chase Cancer Center) for the help with qPCR, Dr. Warren Kruger (Fox Chase Cancer Center) for providing an opportunity to use the Seahorse XF analyzer, and Drs. Erica Golemis and Igor Astsaturov (Fox Chase Cancer Center) for their kind advice on the manuscript preparation.

References

1. Cheng JQ, Lee WC, Klein MA, Cheng GZ, Jhanwar SC, Testa JR. Frequent mutations of NF2 and allelic loss from chromosome band 22q12 in malignant mesothelioma: evidence for a two-hit mechanism of NF2 inactivation. Genes Chromosomes Cancer. 1999; 24:238–42. [PubMed: 10451704]
2. Schroeder RD, Angelo LS, Kurzrock R. NF2/merlin in hereditary neurofibromatosis 2 versus cancer: biologic mechanisms and clinical associations. Oncotarget. 2014; 5:67–77. [PubMed: 24393766]
3. Lallemand D, Curto M, Saotome I, Giovannini M, McClatchey AI. NF2 deficiency promotes tumorigenesis and metastasis by destabilizing adherens junctions. Genes Dev. 2003; 17:1090–100. [PubMed: 12695331]
4. Lallemand D, Saint-Amaux AL, Giovannini M. Tumor-suppression functions of merlin are independent of its role as an organizer of the actin cytoskeleton in Schwann cells. J Cell Sci. 2009 Nov 15.122:4141–9. [PubMed: 19910496]
5. Zhou L, Ercolano E, Ammoun S, Schmid MC, Barczyk MA, Hanemann CO. Merlin-deficient human tumors show loss of contact inhibition and activation of Wnt/β-catenin signaling linked to the PDGFR/Src and Rac/PAK pathways. Neoplasia. 2011; 13:1101–12. [PubMed: 22247700]

6. Pelton PD, Sherman LS, Rizvi TA, Marchionni MA, Wood P, Friedman RA, et al. Ruffling membrane, stress fiber, cell spreading and proliferation abnormalities in human Schwannoma cells. Oncogene. 1998; 17:2195–209. [PubMed: 9811451]
7. Utermark T, Kaempchen K, Hanemann CO. Pathological adhesion of primary human schwannoma cells is dependent on altered expression of integrins. Brain Pathol. 2003; 13:352–63. [PubMed: 12946024]
8. Kissil JL, Johnson KC, Eckman MS, Jacks T. Merlin phosphorylation by p21-activated kinase 2 and effects of phosphorylation on merlin localization. J Biol Chem. 2002; 277:10394–9. [PubMed: 11782491]
9. Xiao GH, Beeser A, Chernoff J, Testa JR. p21-activated kinase links Rac/Cdc42 signaling to merlin. J Biol Chem. 2002; 277:883–6. [PubMed: 11719502]
10. Camacho-Concha N, Olivos-Ortiz A, Nuñez-Rivera A, Pedroza-Saavedra A, Gutierrez-Xicotencatl L, Rosenstein Y, et al. CD43 promotes cells transformation by preventing merlin-mediated contact inhibition of growth. PLoS One. 2013; 8:e80806. [PubMed: 24260485]
11. Kaempchen K, Mielke K, Utermark T, Langmesser S, Hanemann CO. Upregulation of the Rac1/JNK signaling pathway in primary human schwannoma cells. Human Molecular Genetics. 2003; 12:1211–21. [PubMed: 12761036]
12. Li W, You L, Cooper J, Schiavon G, Pepe-Caprio A, Zhou L, et al. Merlin/NF2 suppresses tumorigenesis by inhibiting the E3 ubiquitin ligase CRL4(DCAF1) in the nucleus. Cell. 2010; 140:477–90. [PubMed: 20178741]
13. Hamaratoglu F, Willecke M, Kango-Singh M, Nolo R, Hyun E, Tao C, et al. The tumour-suppressor genes NF2/Merlin and Expanded act through Hippo signalling to regulate cell proliferation and apoptosis. Nat Cell Biol. 2006; 8:27–36. [PubMed: 16341207]
14. McClatchey AI, Giovannini M. Membrane organization and tumorigenesis--the NF2 tumor suppressor, Merlin. Genes Dev. 2005; 19:2265–77. [PubMed: 16204178]
15. Morrison H, Sherman LS, Legg J, Banine F, Isacke C, Haipek CA, et al. The NF2 tumor suppressor gene product, merlin, mediates contact inhibition of growth through interactions with CD44. Genes Dev. 2001; 15:968–80. [PubMed: 11316791]
16. Plotkin SR, Singh MA, O'Donnell CC, Harris GJ, McClatchey AI, Halpin C. Audiologic and radiographic response of NF2-related vestibular schwannoma to erlotinib therapy. Nat Clin Pract Oncol. 2008; 5:487–91. [PubMed: 18560388]
17. Plotkin SR, Stemmer-Rachamimov AO, Barker FGn, Halpin C, Padera TP, Tyrrell A, et al. Hearing improvement after bevacizumab in patients with neurofibromatosis type 2. N Engl J Med. 2009; 361:358–67. [PubMed: 19587327]
18. Ahmad ZK, Brown CM, Cueva RA, Ryan AF, Doherty JK. ErbB expression, activation, and inhibition with lapatinib and tyrphostin (AG825) in human vestibular schwannomas. Otol Neurotol. 2011; 32:841–7. [PubMed: 21659924]
19. Giovannini M, Bonne NX, Vitte J, Chareyre F, Tanaka K, Adams R, et al. mTORC1 inhibition delays growth of neurofibromatosis type 2 schwannoma. Neuro Oncol. 2014; 16:493–504. [PubMed: 24414536]
20. Zhao Y, Butler EB, Tan M. Targeting cellular metabolism to improve cancer therapeutics. Cell Death Dis. 2013; 4:e532. [PubMed: 23470539]
21. Swinnen JV, Heemers H, van de Sande T, de Schrijver E, Brusselmans K, Heyns W, et al. Androgens, lipogenesis and prostate cancer. J Steroid Biochem Mol Biol. 2004; 92:273–9. [PubMed: 15663990]
22. Shiragami R, Murata S, Kosugi C, Tezuka T, Yamazaki M, Hirano A, et al. Enhanced antitumor activity of cerulenin combined with oxaliplatin in human colon cancer cells. Int J Oncol. 2013; 43:431–8. [PubMed: 23754252]
23. Giovannini M, Robanus-Maandag E, van der Valk M, Niwa-Kawakita M, Abramowski V, Goutebroze L, et al. Conditional biallelic Nf2 mutation in the mouse promotes manifestations of human neurofibromatosis type 2. Genes Dev. 2000; 14:1617–30. [PubMed: 10887156]
24. Flavin R, Peluso S, Nguyen PL, Loda M. Fatty acid synthase as a potential therapeutic target in cancer. Future Oncol. 2010; 6:551–62. [PubMed: 20373869]

25. Lupu R, Menendez JA. Pharmacological inhibitors of Fatty Acid Synthase (FASN)--catalyzed endogenous fatty acid biogenesis: a new family of anti-cancer agents. Curr Pharm Biotechnol. 2006; 7:483–93. [PubMed: 17168665]
26. Fritz V, Benfodda Z, Henriquet C, Hure S, Cristol JP, Michel F, et al. Metabolic intervention on lipid synthesis converging pathways abrogates prostate cancer growth. Oncogene. 2013; 32:5101–10. [PubMed: 23208508]
27. Genschel U. Coenzyme A Biosynthesis: Reconstruction of the Pathway in Archaea and an Evolutionary Scenario Based on Comparative Genomics. Mol Biol Evol. 2004; 21:1242–51. [PubMed: 15014152]
28. Vance D, Goldberg I, Mitsuhashi O, Bloch K. Inhibition of fatty acid synthetases by the antibiotic cerulenin. Biochemical and biophysical research communications. 1972; 48:649–56. [PubMed: 4625866]
29. Hardwicke MA, Rendina AR, Williams SP, Moore ML, Wang L, Krueger JA, et al. A human fatty acid synthase inhibitor binds beta-ketoacyl reductase in the keto-substrate site. Nature chemical biology. 2014; 10:774–9. [PubMed: 25086508]
30. Bauerschlag DO, Maass N, Leonhardt P, Verburg FA, Pecks U, Zeppernick F, et al. Fatty acid synthase overexpression: target for therapy and reversal of chemoresistance in ovarian cancer. Journal of translational medicine. 2015; 13
31. Funabashi H, Kawaguchi A, Tomoda H, Omura S, Okuda S, Iwasaki S. Binding site of cerulenin in fatty acid synthetase. Journal of biochemistry. 1989; 105:751–5. [PubMed: 2666407]
32. Price AC, Choi KH, Heath RJ, Li Z, White SW, Rock CO. Inhibition of beta-ketoacyl-acyl carrier protein synthases by thiolactomycin and cerulenin. Structure and mechanism. J Biol Chem. 2001; 276:6551–9. [PubMed: 11050088]
33. Slabaugh MB, Leonard JM, Knapp SJ. Condensing enzymes from Cuphea wrightii associated with medium chain fatty acid biosynthesis. Plant J. 1998; 13:611–20. [PubMed: 9681003]
34. Pizer ES, Thupari J, Han WF, Pinn ML, Chrest FJ, Frehywot GL, et al. Malonyl-coenzyme-A is a potential mediator of cytotoxicity induced by fatty-acid synthase inhibition in human breast cancer cells and xenografts. Cancer research. 2000; 60:213–8. [PubMed: 10667561]
35. Thupari JN, Pinn ML, Kuhajda FP. Fatty acid synthase inhibition in human breast cancer cells leads to malonyl-CoA-induced inhibition of fatty acid oxidation and cytotoxicity. Biochemical and biophysical research communications. 2001; 285:217–23. [PubMed: 11444828]
36. Menendez JA, Lupu R. Fatty acid synthase and the lipogenic phenotype in cancer pathogenesis. Nature reviews Cancer. 2007; 7:763–77. [PubMed: 17882277]
37. Kudo N, Barr AJ, Barr RL, Desai S, Lopaschuk GD. High rates of fatty acid oxidation during reperfusion of ischemic hearts are associated with a decrease in malonyl-CoA levels due to an increase in 5′-AMP-activated protein kinase inhibition of acetyl-CoA carboxylase. J Biol Chem. 1995; 270:17513–20. [PubMed: 7615556]
38. Garcia-Villafranca J, Castro J. Effects of 5-iodotubercidin on hepatic fatty acid metabolism mediated by the inhibition of acetyl-CoA carboxylase. Biochemical pharmacology. 2002; 63:1997–2000. [PubMed: 12093476]
39. Fullerton MD, Galic S, Marcinko K, Sikkema S, Pulinilkunnil T, Chen ZP, et al. Single phosphorylation sites in Acc1 and Acc2 regulate lipid homeostasis and the insulin-sensitizing effects of metformin. Nature medicine. 2013; 19:1649–54.
40. Horton JD, Goldstein JL, Brown MS. SREBPs: activators of the complete program of cholesterol and fatty acid synthesis in the liver. J Clin Invest. 2002; 109:1125–31. [PubMed: 11994399]
41. Pandey PR, Xing F, Sharma S, Watabe M, Pai SK, Iiizumi-Gairani M, et al. Elevated lipogenesis in epithelial stem-like cell confers survival advantage in ductal carcinoma in situ of breast cancer. Oncogene. 2013; 32:5111–22. [PubMed: 23208501]
42. Péterfy M, Phan J, Xu P, Reue K. Lipodystrophy in the fld mouse results from mutation of a new gene encoding a nuclear protein, lipin. Nat Genet. 2001; 27:121–4. [PubMed: 11138012]
43. Phan J, Reue K. Lipin, a lipodystrophy and obesity gene. Cell Metab. 2005; 1:73–83. [PubMed: 16054046]
44. James MF, Han S, Polizzano C, Plotkin SR, Manning BD, Stemmer-Rachamimov AO, et al. NF2/merlin is a novel negative regulator of mTOR complex 1, and activation of mTORC1 is associated

with meningioma and schwannoma growth. Mol Cell Biol. 2009; 29:4250–61. [PubMed: 19451225]

45. Porstmann T, Santos CR, Griffiths B, Cully M, Wu M, Leevers S, et al. SREBP activity is regulated by mTORC1 and contributes to Akt-dependent cell growth. Cell Metab. 2008; 8:224–36. [PubMed: 18762023]
46. Yuan M, Pino E, Wu L, Kacergis M, Soukas AA. Identification of Akt-independent regulation of hepatic lipogenesis by mammalian target of rapamycin (mTOR) complex 2. J Biol Chem. 2012; 287:29579–88. [PubMed: 22773877]
47. Loftus TM, Jaworsky DE, Frehywot GL, Townsend CA, Ronnett GV, Lane MD, et al. Reduced food intake and body weight in mice treated with fatty acid synthase inhibitors. Science. 2000; 288:2379–81. [PubMed: 10875926]
48. Menendez JA, Mehmi I, Verma VA, Teng PK, Lupu R. Pharmacological inhibition of fatty acid synthase (FAS): a novel therapeutic approach for breast cancer chemoprevention through its ability to suppress Her-2/neu (erbB-2) oncogene-induced malignant transformation. Mol Carcinog. 2004; 41:164–78. [PubMed: 15390078]
49. Gabrielson EW, Pinn ML, Testa JR, Kuhajda FP. Increased fatty acid synthase is a therapeutic target in mesothelioma. Clinical cancer research: an official journal of the American Association for Cancer Research. 2001; 7:153–7. [PubMed: 11205903]
50. Haase D, Schmidl S, Ewald C, Kalff R, Huebner C, Firsching R, et al. Fatty acid synthase as a novel target for meningioma therapy. Neuro Oncol. 2010; 12:844–54. [PubMed: 20511185]
51. Rossato FA, Zecchin KG, La Guardia PG, Ortega RM, Alberici LC, Costa RA, et al. Fatty Acid synthase inhibitors induce apoptosis in non-tumorigenic melan-a cells associated with inhibition of mitochondrial respiration. PLoS One. 2014; 9:e101060. [PubMed: 24964211]
52. Wang TF, Wang H, Peng AF, Luo QF, Liu ZL, Zhou RP, et al. Inhibition of fatty acid synthase suppresses U-2 OS cell invasion and migration via downregulating the activity of HER2/PI3K/AKT signaling pathway in vitro. Biochemical and biophysical research communications. 2013; 440:229–34. [PubMed: 24041695]
53. Thupari JN, Landree LE, Ronnett GV, Kuhajda FP. C75 increases peripheral energy utilization and fatty acid oxidation in diet-induced obesity. Proceedings of the National Academy of Sciences of the United States of America. 2002; 99:9498–502. [PubMed: 12060712]
54. Swinnen JV, Brusselmans K, Verhoeven G. Increased lipogenesis in cancer cells: new players, novel targets. Curr Opin Clin Nutr Metab Care. 2006; 9:358–65. [PubMed: 16778563]
55. Sekido Y. Molecular pathogenesis of malignant mesothelioma. Carcinogenesis. 2013; 34:1413–9. [PubMed: 23677068]
56. Tahiliani AG, Beinlich CJ. Pantothenic acid in health and disease. Vitamins and hormones. 1991; 46:165–228. [PubMed: 1746161]

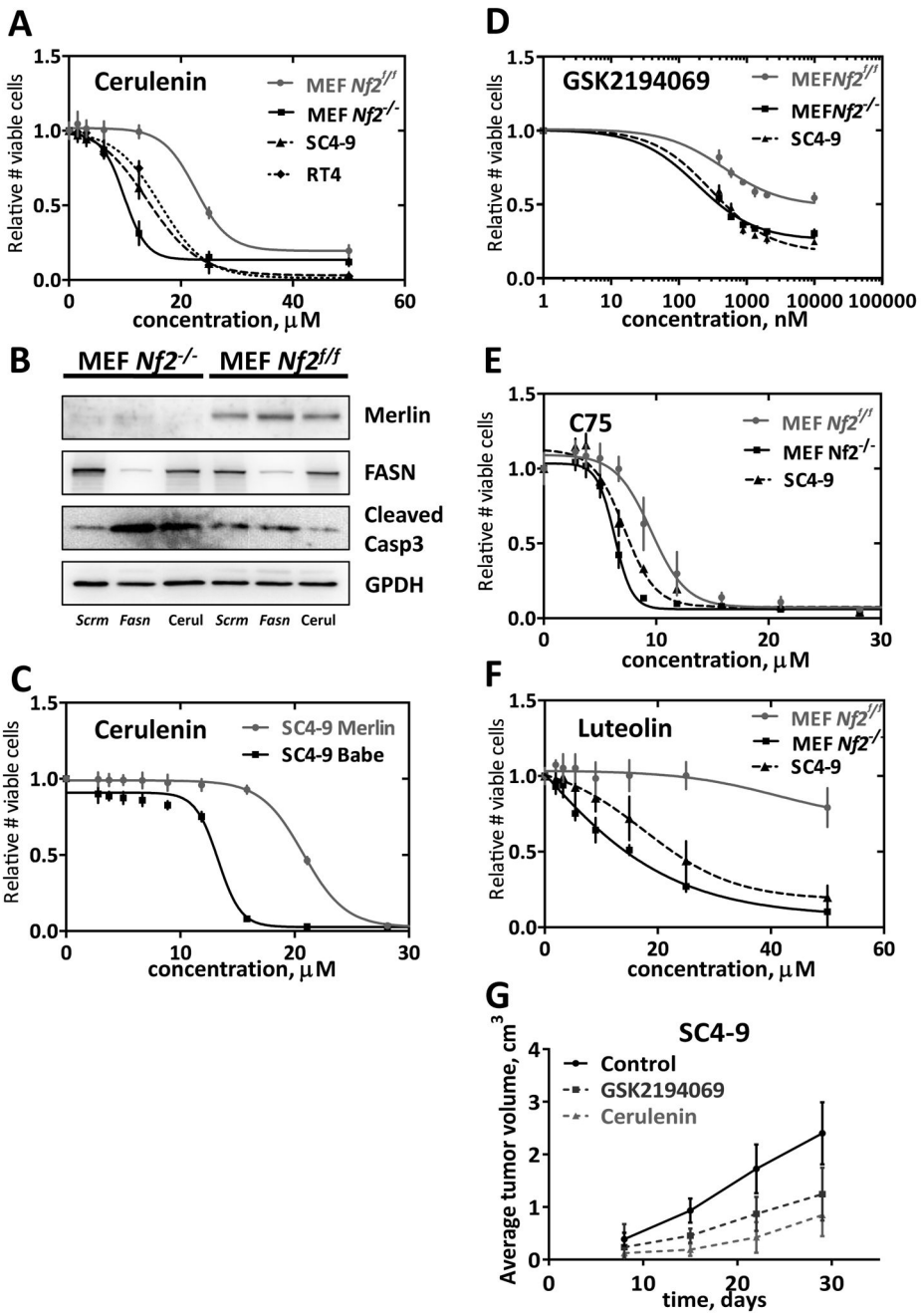

Figure 1. Effects of FASN inhibition

A) Cerulenin dose response curve in *Nf2*$^{-/-}$ and *Nf2*$^{f/f}$ MEFs, SC4–9 and RT4 cells. Cells were treated with the indicated amounts of cerulenin for 48 hr. Experiments were done in quadruplicates and repeated 4 times. Alamar Blue was used for read-outs. Mean values and 95% confidence intervals are shown on graphs. **B)** Increased Casp3 cleavage in *Nf2*$^{-/-}$ MEFs transfected with anti-*Fasn* siRNA. Cells were transfected by electroporation with anti-*Fasn* and scrambled (negative control) siRNAs, final concentration 100 nM, and plated into 6-well plates (250,000 cells/well). **C)** Effect of reintroducing Merlin in *Nf2*-deficient schwannoma cells. SC4–9 mouse schwannoma cells, transiently transfected with empty

pBabe-puro plasmid or pBabe-Merlin plasmid, were tested for sensitivity to cerulenin. All experiments were done in quadruplicates and repeated 4 times. Alamar Blue was used for read-outs. Mean values and 95% confidence intervals are shown on graphs. At 24 h post-transfection, lysates were analyzed by immunoblotting using rabbit anti-FASN and anti-cleaved Casp3 antibodies. Typical blots are shown. Band intensities were quantified using ImageJ software and normalized to GAPDH band intensities. All experiments were repeated 3 times. Mean values and 95% confidence intervals are shown on graphs. **** − $p \leq 0.0001$. **D–F)** Effects of FASN inhibitors GSK2194069, C75, and Luteolin. Experiments were done using the indicated cell types in quadruplicate and repeated 4 times. Alamar Blue was used for read-outs. Mean values and 95% confidence intervals are shown on graphs. **G**) *In vivo* effects of cerulenin. $3x10^6$ SC4–9 cells in matrigel:PBS 1:1 per mouse (female *nu/nu*) were injected subcutaneously. 30 mg/kg/day of cerulenin or 3 mg/kg/day of GSK2194069 in corn oil were given by oral gavage daily starting day 3 after injection; n = 6. Mean values and 95% confidence intervals are shown on graphs.

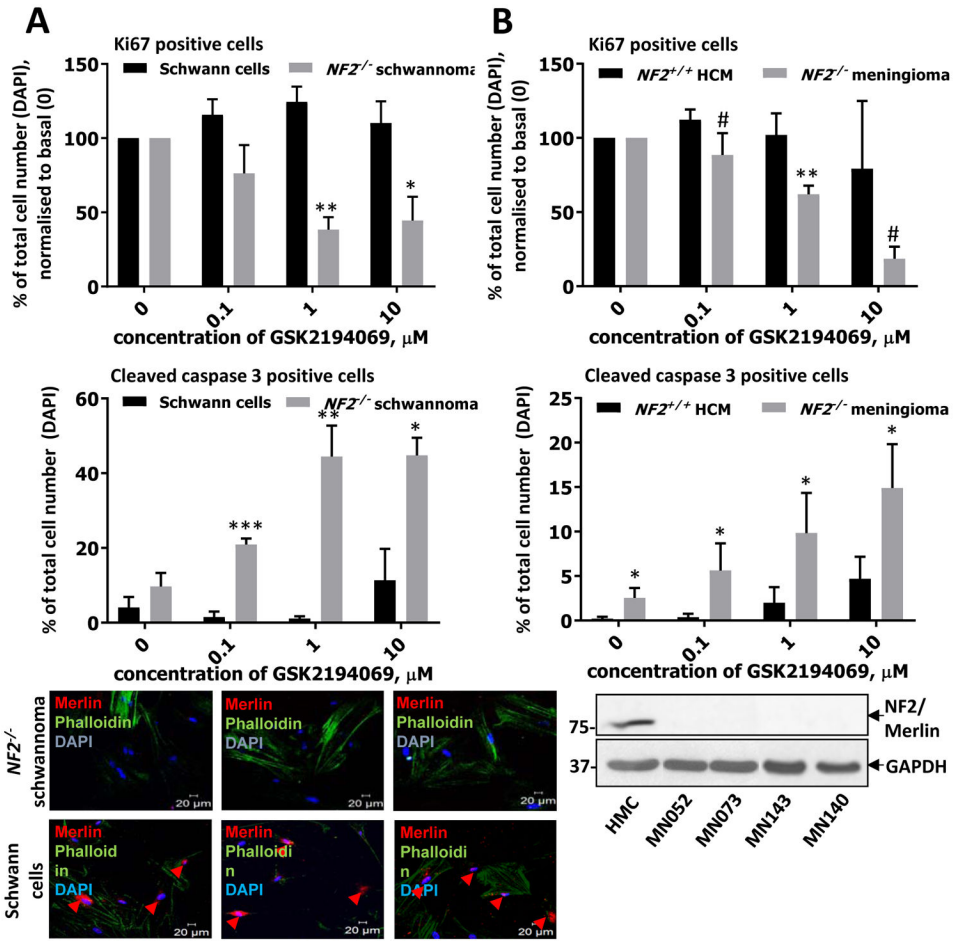

Figure 2. Effects of FASN inhibitors in human schwannoma and meningioma cells

A) Dose response to FASN inhibitors in primary human schwannoma cells ($NF2^{-/-}$) compared to normal Schwann cells ($NF2^{+/+}$). Cells were incubated with indicated concentrations of GSK2194069 for 72 hours. Proliferation (Ki67, first panel), apoptosis (cleaved Casp3, second panel) and merlin status (third panel), were confirmed by immunocytochemistry and confocal microscopy using DAPI for the total cell count and phalloidin for cytoskeleton staining. Quantification of proliferation and apoptosis was performed using ZEN software. B) Dose response in primary human meningioma cells ($NF2^{-/-}$) to GSK2194069 compared to normal meningeal cells ($NF2^{+/+}$). Cells were incubated with indicated concentrations of GSK2194069 for 72 hours, proliferation (Ki67, first panel) and apoptosis (cleaved Casp3, second panel) were confirmed by immunocytochemistry using DAPI for the total cell count, merlin status was confirmed by immunoblotting third panel). Experiments were performed in at least triplicates using at least three independent batches of cells from different individuals. # − $0.05 < p < 0.07$, * − $p < 0.05$; ** − $p < 0.01$. Mean ± s.e.m. is shown on graph.

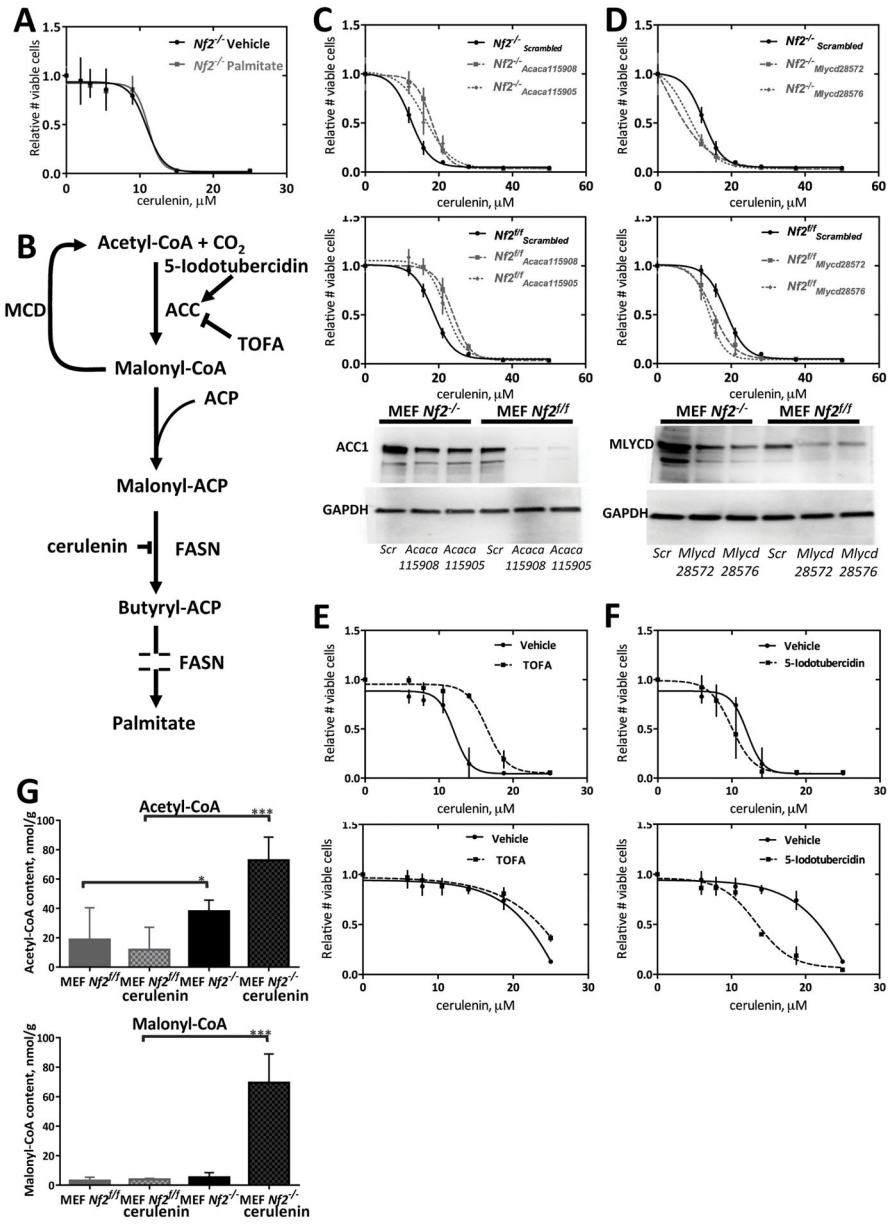

Figure 3. Modulation of the effect of cerulenin by genetic and chemical modulation of acetyl-CoA carboxylase (ACC1) and malonyl-CoA decarboxylase (MCD) activity

A) Supplementing culture media with palmitate does not reverse the effect of cerulenin. Palmitate sodium salt (5 μM) was added together with the indicated concentrations of cerulenin, 4 hours after cell seeding, and cells were then incubated for 48 hours. An experiment was done in quadruplicate and repeated 4 times. Mean values and 95% confidence intervals are shown on graphs. **B)** Cartoon of Palmitate synthetic pathway. Sites of action of small molecule inhibitors are indicated. ACC = acetyl-CoA carboxylase, MCD = malonyl-CoA decarboxylase, ACP = acyl carrier protein, FASN = fatty acid synthase, TOFA = tetradecyloxyfuroic acid. **C)** Effect of *Acaca* knockdown on FASN inhibition. Cells were transfected by electroporation with anti-*Acaca* and scrambled (negative control) siRNAs. The indicated amounts of cerulenin were added in 24 hours and incubated for 48

hours. Parallel transfections for knockdown control were done in a 6-well format. Experiments were done in quadruplicates and repeated 3 times. Mean values and 95% confidence intervals are shown on graphs. **D)** Effect of *Mlycd* knockdown on FASN inhibition. Cells were transfected by electroporation with anti-*Mlycd* and scrambled (negative control) siRNAs. Indicated amounts of cerulenin were added in 24 hours and incubated for 48 hours. Parallel transfections for knockdown control were done in a 6-well format. Experiments were done in quadruplicates and repeated 4 times. Mean values and 95% confidence intervals are shown on graphs. **E)** Effect of chemical inhibition of ACC on cerulenin toxicity. The ACC inhibitor TOFA (25 μM) was added together with the indicated concentrations of cerulenin, 4 hours after cell seeding, and cells were then incubated for 48 hours. **F)** Effect of chemical activation of ACC on cerulenin toxicity. The ACC activator 5-iodotubericidin (2.5 μM) was added together with the indicated concentrations of cerulenin, 4 hours after cell seeding, and cells were then incubated for 48 hours. All experiments were done in quadruplicates and repeated 3 times. Mean values and 95% confidence intervals are shown on graphs. **G)** Effects of Merlin on acyl-CoA levels. UPLC-MS/MS measurements of acetyl-CoA and malonyl-CoA. MEFs were treated with 0.1 μL/mL DMSO or 5 μM cerulenin for 24 hours. Experiments were repeated 3 times. Mean values and 95% confidence intervals are shown on graphs. * − $p \leq 0.05$, *** − $p \leq 0.001$.

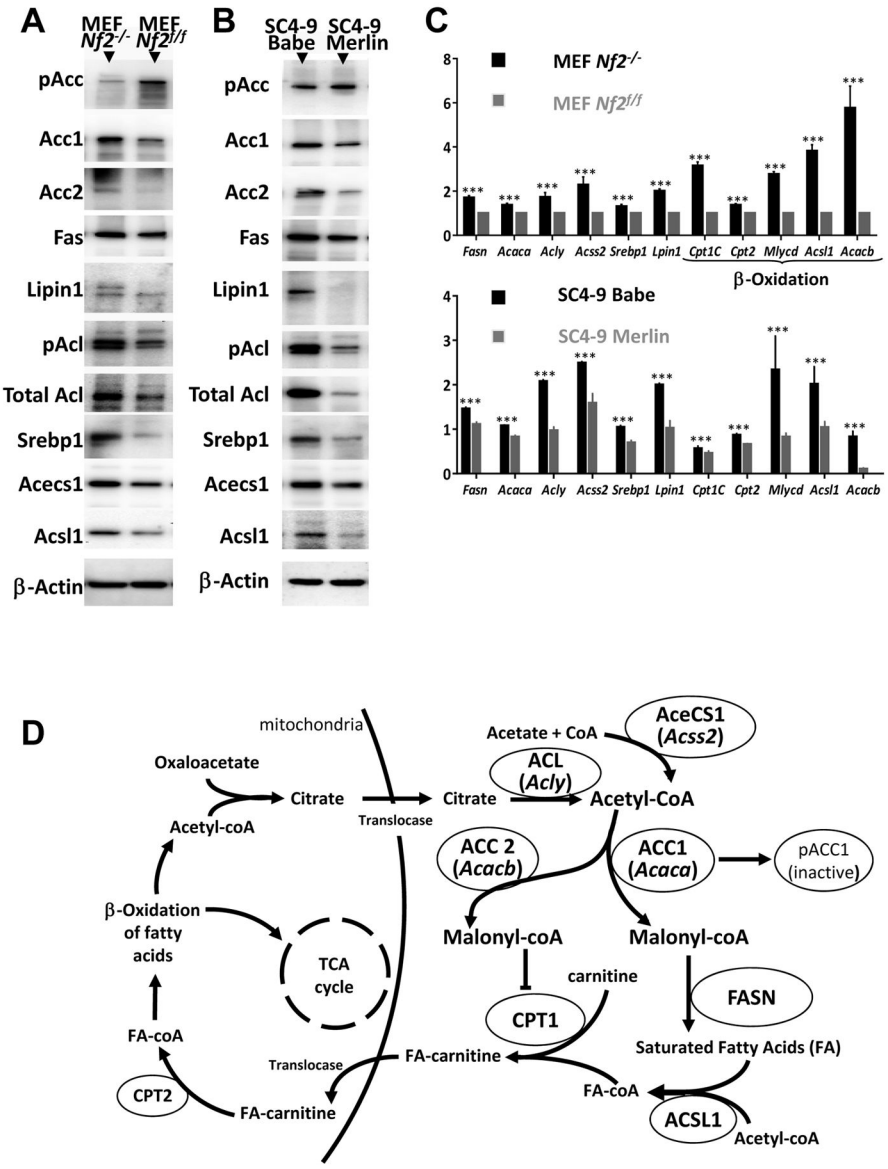

Figure 4. Effects of Merlin on lipogenesis-related gene expression

A) Immunoblot detection of levels of expression and phosphorylation of lipogenesis-related proteins in *Nf2*$^{-/-}$ and *Nf2*$^{f/f}$ MEFs. B) Immunoblot detection of levels of expression and phosphorylation of lipogenesis-related proteins in SC4–9 Babe (SC4–9 cells transiently transfected with empty pBabe-puro plasmid); SC4–9 Merlin (SC4–9 cells transiently transfected with pBabe-Merlin plasmid). Typical blots are shown. C) Lipogenesis gene expression quantification by qPCR. RNA quantification was performed on *Nf2*$^{-/-}$ and *Nf2*$^{f/f}$ MEFs; SC4–9 Babe (SC4–9 cells transiently transfected with empty pBabe-puro plasmid); SC4–9 Merlin (SC4–9 cells transiently transfected with pBabe-Merlin plasmid); and *Nf2*$^{-/-}$ (FH912) and *Nf2*$^{f/f}$ (FC912) mouse Schwann cells. All experiments were repeated 4 times Mean and 95% CI are shown on graphs. *** − $p \leq 0.001$. D) Enzymes involved in fatty acid sythesis. ACC1, *Acaca* = Acetyl-CoA carboxylase 1; ACC2, *Acacb* = Acetyl-CoA carboxylase 2; ACL = ATP citrate lyase; SREBP1 = Sterol regulatory element binding

protein 1. ACECS1, *Acss2* = Acetyl-CoA synthase 1; ACSL1 = Acyl-CoA synthetase long-chain family member 1. *Cpt1c* = Carnitine palmitoyl transferase Ic. *Cpt2* = Carnitine palmitoyl transferase II. *Mlycd* = Malonyl-CoA decarboxylase.

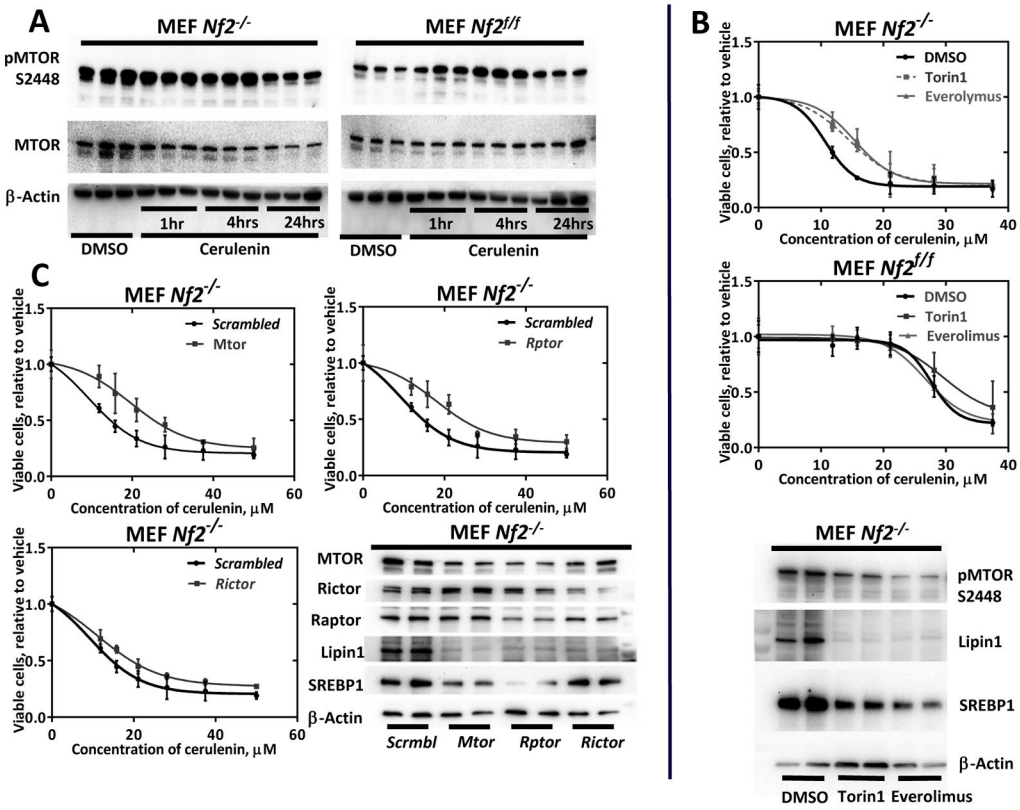

Figure 5. Role of TORC1 in lipogenesis upregulation in *Nf2*$^{-/-}$ MEFs

A) Immunoblot detection of MTOR activation in *Nf2*$^{-/-}$ *vs Nf2*$^{f/f}$ MEFs. B) Effect of chemical inhibition of MTOR on cerulenin toxicity. The TORC1 and TORC2 inhibitor Torin1 (25 nM) or TORC1 inhibitor Everolimus (100 nM) were added together with the indicated concentrations of cerulenin, 4 hours after cell seeding, and cells were then incubated for 48 hours. C) *Mtor*, *Rptor* and *Rictor* siRNA transfections. Cells were transfected by electroporation with anti-*Mtor*, *Rptor* or *Rictor* and scrambled (negative control) siRNAs. The indicated amounts of cerulenin were added in 24 hours and incubated for 48 hours. All experiments were repeated 2 times, dose response curves were done in quadruplicates, and for WBs each lysate type was run in duplicates for transfer consistency control. Mean values and 95% confidence intervals are shown on graphs.

Table 1

Tricarbonic acid cycle and glycolysis metabolite level alteration in *Nf2*-deficient cells

Levels of metabolites as measured by gas chromatography and high performance liquid chromatography. Bolded, underlined numbers indicate significant differences ($p \leq 0.05$) between the groups shown, metabolite ratio of <1.00. Greyed, underlined boxes indicate significant difference ($p \leq 0.05$) between the groups shown; metabolite ratio of ≥ 1.00. Two-tailed Welch's *t*-test was used to compare FH912 and FC912 cells, $n = 5$. Two-way ANOVA contrasts were used to compare *$Nf2^{-/-}$ and $Nf2^{f/f}$ MEFs and to evaluate cerulenin treatment effects.*

Super Pathway	Sub Pathway	Biochemical Name	Fold change	
			Two-Way ANOVA Contrasts	Welch's Two-Sample *t*-Test
			$\frac{\text{MEF } Nf2^{-/-}}{\text{MEF } Nf2^{f/f}}$	$\frac{\text{FH912}}{\text{FC912}}$
Energy	TCA Cycle	citrate	**1.47**	**0.45**
		succinate	**2.62**	1.56
		fumarate	**1.23**	**0.47**
		malate	**1.94**	**0.33**
	Oxidative Phosphorylation	acetylphosphate	**1.8**	**0.45**
		pyrophosphate	0.81	0.78
		phosphate	1.01	**0.74**
	Glycolysis, Gluconeogenesis, and Pyruvate Metabolism	glucose	**0.32**	1.45
		glucose-6-phosphate	0.74	**0.05**
		glucose 1-phosphate	1.12	0.68
		fructose-6-phosphate	0.82	**0.16**
		3-phosphoglycerate	**0.12**	0.52
		pyruvate	**0.56**	**1.59**
		lactate	1.13	1.1
		glycerate	**0.35**	0.89

Table 2
Upregulation of Fatty Acid Synthesis in *Nf2*-deficient cells

Samples were processed and analyzed as in Table 1.

Super Pathway	Sub Pathway	Biochemical Name	Fold change	
			Two-Way ANOVA Contrasts	Welch's Two-Sample *t*-Test
			$\frac{\text{MEF } Nf2^{-/-}}{\text{MEF } Nf2^{f/f}}$	$\frac{\text{FH912}}{\text{FC912}}$
Lipid Metabolism	Long Chain Fatty Acids	margarate (17:0)	**1.2**	**1.35**
		10-heptadecenoate (17:1n7)	1.08	**1.49**
		stearate (18:0)	**1.17**	**1.33**
		nonadecanoate (19:0)	**1.91**	1.14
		10-nonadecenoate (19:1n9)	**1.26**	**2.76**
		arachidate (20:0)	**1.41**	**1.82**
		eicosenoate (20:1n9 or 11)	0.93	**2.78**
		erucate (22:1n9)	0.92	**2.67**
		nervonate (24:1n9)	0.87	**2.88**
	Polyunsaturated	stearidonate (18:4n3)	**3.09**	1
	Fatty Acid	eicosapentaenoate (20:5n3)	**1.41**	1
	(n3 and n6)	docosapentaenoate (22:5n3)	**1.85**	**1.46**
		docosahexaenoate (22:6n3)	**1.66**	**1.97**
		docosatrienoate (22:3n3)	**0.59**	**1.63**
		linoleate (18:2n6)	0.95	**2.21**
		linolenate (18:3n3 or 6)	1.12	**2**
		dihomo-linolenate (20:3n3/n6)	**1.79**	**0.49**
		arachidonate (20:4n6)	**1.58**	**1.92**
		docosadienoate (22:2n6)	**0.74**	**2.49**
		dihomo-linoleate (20:2n6)	0.82	**2.51**
	Fatty Acid, Branched	15-methylpalmitate	**1.41**	1.08
		17-methylstearate	**1.28**	**2.1**